SUPPORTING INFORMATION

Discrete Heterogeneous Quaternary Structure Formed by α/β-Peptide Foldamers and α-Peptides

Joshua L. Price, W. Seth Horne, and Samuel H. Gellman

Department of Chemistry, University of Wisconsin, 1101 University Ave., Madison, WI 53706

α-peptide **1**	AQLEKELQALEKELAQLEWELQALEKELAQ
α-peptide **2**	AQLKKKLQALKKKLAQLKWKLQALKKKLAQ
α-peptide **4**	AQLEKENQALEKELAQLEWELQALEKELAQ
α/β-peptide **3**	$\mathbf{X}^{\beta}$L$\mathbf{Z}^{\beta}$K$\mathbf{Z}^{\beta}$L$\mathbf{X}^{\beta}$A$\mathbf{L}_{\mathbf{2}}^{\beta}K\mathbf{Z}^{\beta}K\mathbf{L}_{\mathbf{2}}^{\beta}A\mathbf{X}^{\beta}L\mathbf{Z}^{\beta}W\mathbf{Z}^{\beta}L\mathbf{X}^{\beta}A\mathbf{L}_{\mathbf{2}}^{\beta}K\mathbf{Z}^{\beta}K\mathbf{L}_{\mathbf{2}}^{\beta}A\mathbf{X}^{\beta}$
α/β-peptide **5**	$\mathbf{X}^{\beta}$L$\mathbf{Z}^{\beta}$K$\mathbf{Z}^{\beta}$N$\mathbf{X}^{\beta}$A$\mathbf{L}_{\mathbf{2}}^{\beta}K\mathbf{Z}^{\beta}K\mathbf{L}_{\mathbf{2}}^{\beta}A\mathbf{X}^{\beta}L\mathbf{Z}^{\beta}W\mathbf{Z}^{\beta}L\mathbf{X}^{\beta}A\mathbf{L}_{\mathbf{2}}^{\beta}K\mathbf{Z}^{\beta}K\mathbf{L}_{\mathbf{2}}^{\beta}A\mathbf{X}^{\beta}$
α/β-peptide **6**	$\mathbf{X}^{\beta}$L$\mathbf{Z}^{\beta}$K$\mathbf{Z}^{\beta}$N$\mathbf{X}^{\beta}$A$\mathbf{L}_{\mathbf{3}}^{\beta}K\mathbf{Z}^{\beta}K\mathbf{L}_{\mathbf{3}}^{\beta}A\mathbf{X}^{\beta}L\mathbf{Z}^{\beta}W\mathbf{Z}^{\beta}L\mathbf{X}^{\beta}A\mathbf{L}_{\mathbf{3}}^{\beta}K\mathbf{Z}^{\beta}K\mathbf{L}_{\mathbf{3}}^{\beta}A\mathbf{X}^{\beta}$
α/β-peptide **7**	$\mathbf{X}^{\beta}$L$\mathbf{K}_{\mathbf{3}}^{\beta}K\mathbf{K}_{\mathbf{3}}^{\beta}N\mathbf{X}^{\beta}A\mathbf{L}_{\mathbf{2}}^{\beta}K\mathbf{K}_{\mathbf{3}}^{\beta}K\mathbf{L}_{\mathbf{2}}^{\beta}A\mathbf{X}^{\beta}L\mathbf{K}_{\mathbf{3}}^{\beta}W\mathbf{K}_{\mathbf{3}}^{\beta}L\mathbf{X}^{\beta}A\mathbf{L}_{\mathbf{2}}^{\beta}K\mathbf{K}_{\mathbf{3}}^{\beta}K\mathbf{L}_{\mathbf{2}}^{\beta}A\mathbf{X}^{\beta}$

Figure S1. Sequences of α- and α/β-peptides. Non-bold letters represent α-amino acids according to the standard one-letter code. Bold letters represent β-amino acids, using the following abbreviations: $\mathbf{X}^{\beta}$ = ACPC, $\mathbf{Z}^{\beta}$ = APC, $\mathbf{L}_{\mathbf{2}}^{\beta}$ = β^2-homoleucine, $\mathbf{L}_{\mathbf{3}}^{\beta}$ = β^3-homoleucine, $\mathbf{K}_{\mathbf{3}}^{\beta}$ = β^3-homolysine. α-peptide **4** is the Leu→Asn mutant of α-peptide **1** at position 7. α/β-peptide **5** is the analogous Leu→Asn mutant of α/β-peptide **3** at position 6. α/β-peptide **6** is the constitutional isomer of **5** in which each β^2-homoleucine residue has been replaced with β^3-homoleucine, which shifts the isobutyl side-chain one carbon atom toward the N-terminus of the peptide.

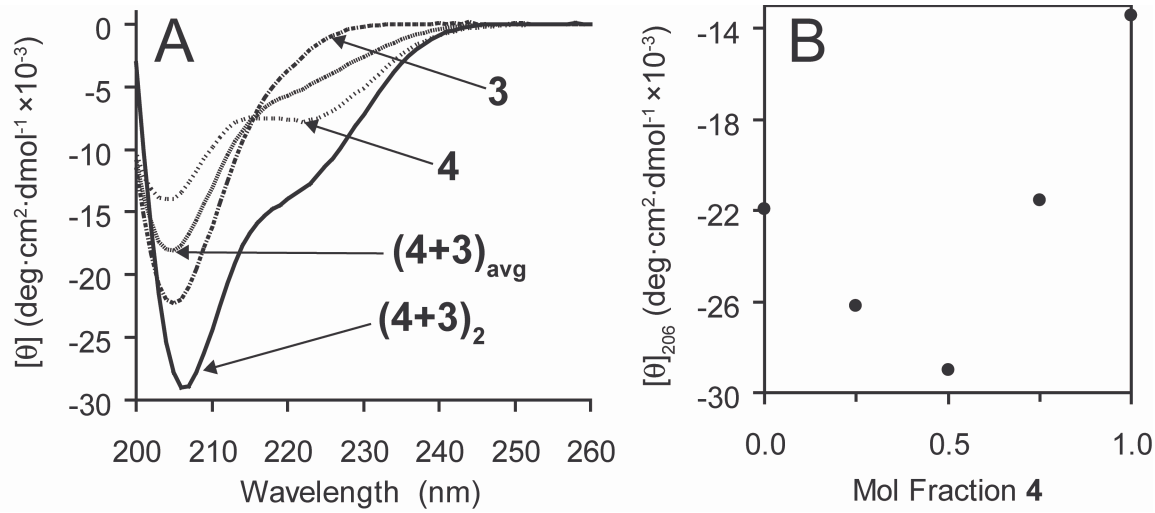

Figure S2. (A) CD spectra of 100 μM α-peptide **4**, 100 μM α/β-peptide **3**, and 50 μM **4** + 50 μM **3** **(4+3)$_2$** in PBS at 25 °C. **(4+3)$_{avg}$** is the average of the CD spectra of **4** alone plus **3** alone. The spectrum of **4** is characteristic of a partially folded α-helical peptide (ref S1), and the spectrum of **3** is consistent with α/β-peptide helicity (for interpretation of CD data from helical α/β-peptides, see ref. S2). The spectrum for **(4+3)$_2$** is more intense than **(4+3)$_{avg}$**, which suggests that **4** and **3** associate in a way that promotes helical folding. (B) Job plot of $[\theta]_{206}$ for 100 μM solutions differing in relative amounts of **4** and **3**, indicating 1:1 stoichiometry in the **4+3** assembly.

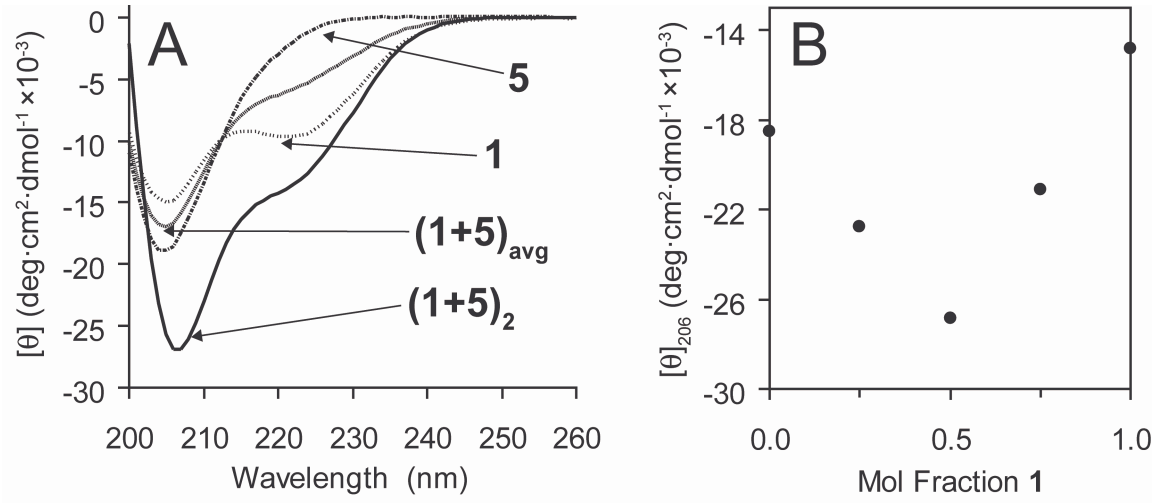

Figure S3. (A) CD spectra of 100 μM α-peptide **1**, 100 μM α/β-peptide **5**, and 50 μM **1** + 50 μM **5** **(1+5)$_2$** in PBS at 25 °C. **(1+5)$_{avg}$** is the average of the CD spectra of **1** alone plus **5** alone. The spectrum of **1** is characteristic of a partially folded α-helical peptide (ref S1), and the spectrum of **5** is consistent with α/β-peptide helicity (for interpretation of CD data from helical α/β-peptides, see ref. S2). The spectrum for **(1+5)$_2$** is more intense than **(1+5)$_{avg}$**, which suggests that **1** and **5** associate in a way that promotes helical folding. (B) Job plot of $[\theta]_{206}$ for 100 μM solutions differing in relative amounts of **1** and **5**, indicating 1:1 stoichiometry in the **1+5** assembly.

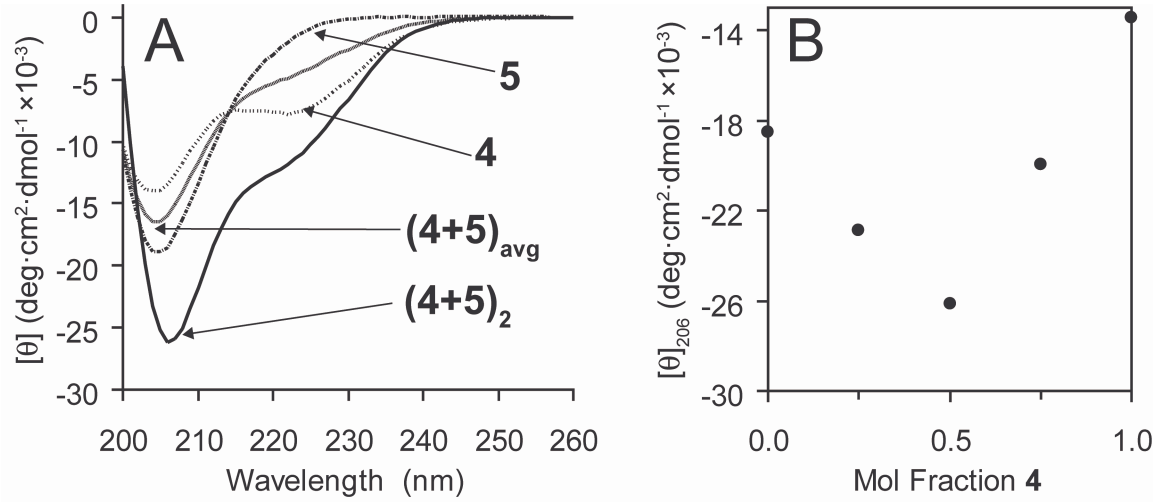

Figure S4. (A) CD spectra of 100 μM α-peptide **4**, 100 μM α/β-peptide **5**, and 50 μM **4** + 50 μM **5** **(4+5)$_2$** in PBS at 25 °C. **(4+5)$_{avg}$** is the average of the CD spectra of **4** alone plus **5** alone. The spectrum of **4** is characteristic of a partially folded α-helical peptide (ref S1), and the spectrum of **3** is consistent with α/β-peptide helicity (for interpretation of CD data from helical α/β-peptides, see ref. S2). The spectrum for **(4+5)$_2$** is more intense than **(4+5)$_{av}$** which suggests that **4** and **5** associate in a way that promotes helical folding. (B) Job plot of $[\theta]_{206}$ for 100 μM solutions differing in relative amounts of **4** and **5**, indicating 1:1 stoichiometry in the **(4+5)$_2$** assembly.

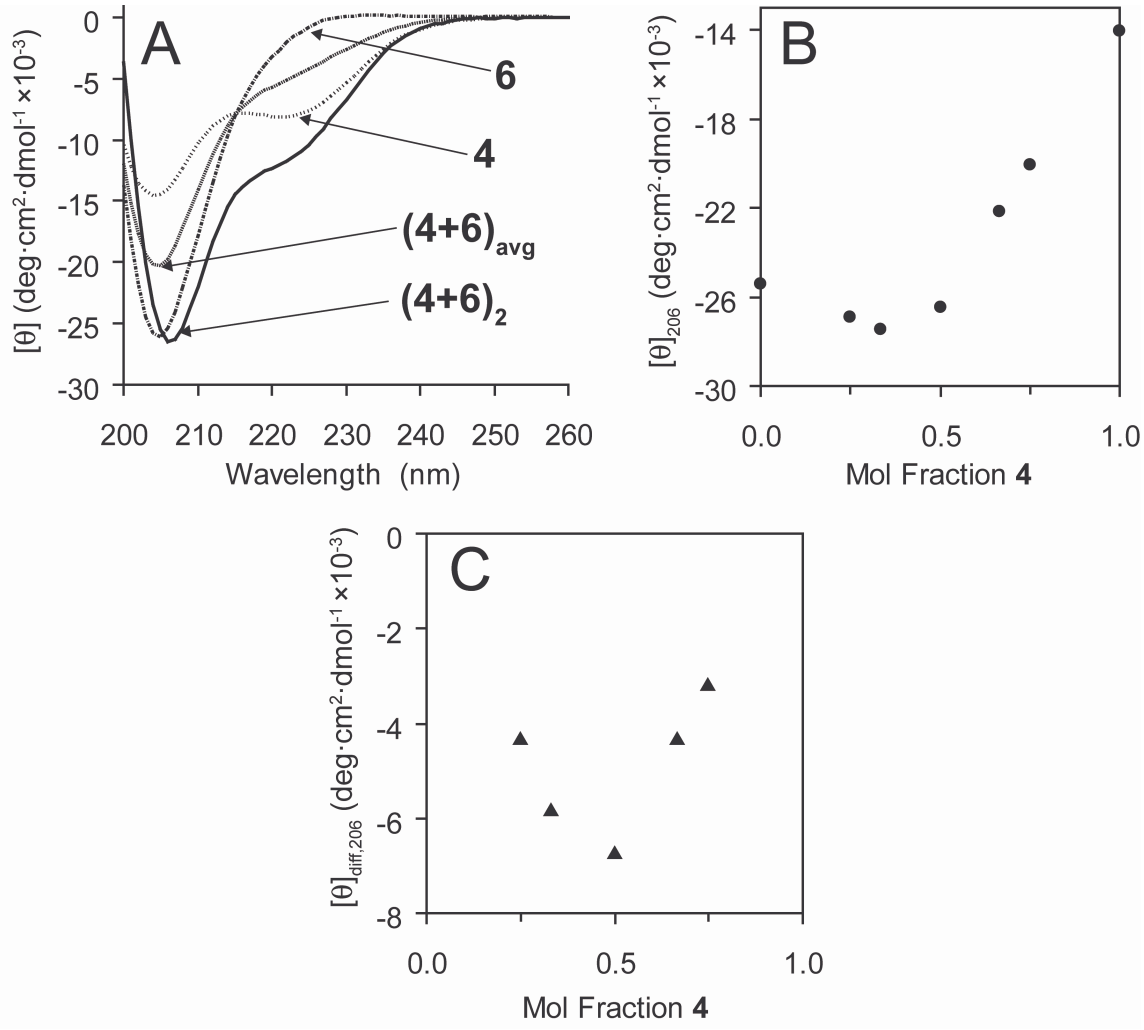

Figure S5. (A) CD spectra of 100 μM α-peptide **4**, 100 μM α/β-peptide **6**, and 50 μM **4** + 50 μM **6** $\mathbf{(4+6)_2}$ in PBS at 25 °C. $\mathbf{(4+6)_{avg}}$ is the average of the CD spectra of **4** alone plus **6** alone. The spectrum of **4** is characteristic of a partially folded α-helical peptide (ref S1), and the spectrum of **6** is consistent with α/β-peptide helicity (for interpretation of CD data from helical α/β-peptides, see ref. S2). The spectrum for $\mathbf{(4+6)_2}$ is more intense than $\mathbf{(4+6)_{avg}}$ which suggests that **4** and **6** associate in a way that promotes helical folding. (B) Job plot of $[\theta]_{206}$ for 100 μM solutions differing in relative amounts of **4** and **6**. (C) Job plot of the difference between the observed $[\theta]_{206}$ and the weighted average $[\theta]_{206}$ (average obtained according to the following equation: $[\theta]_{206,avg} = [\theta]_{206,\,\mathbf{4}} \times$ mol fr **4** + $[\theta]_{206,\,\mathbf{6}} \times$ mol fr **6**) for each mixture of **4** and **6**. This difference provides a measure of the helical structure that is induced by mixing **4** and **6** together. The minimum at 0.5 mole fraction **4** indicates maximum induced helical structure when **4** and **6** are mixed in a 1:1 ratio, suggesting 1:1 stoichiometry in the assembly.

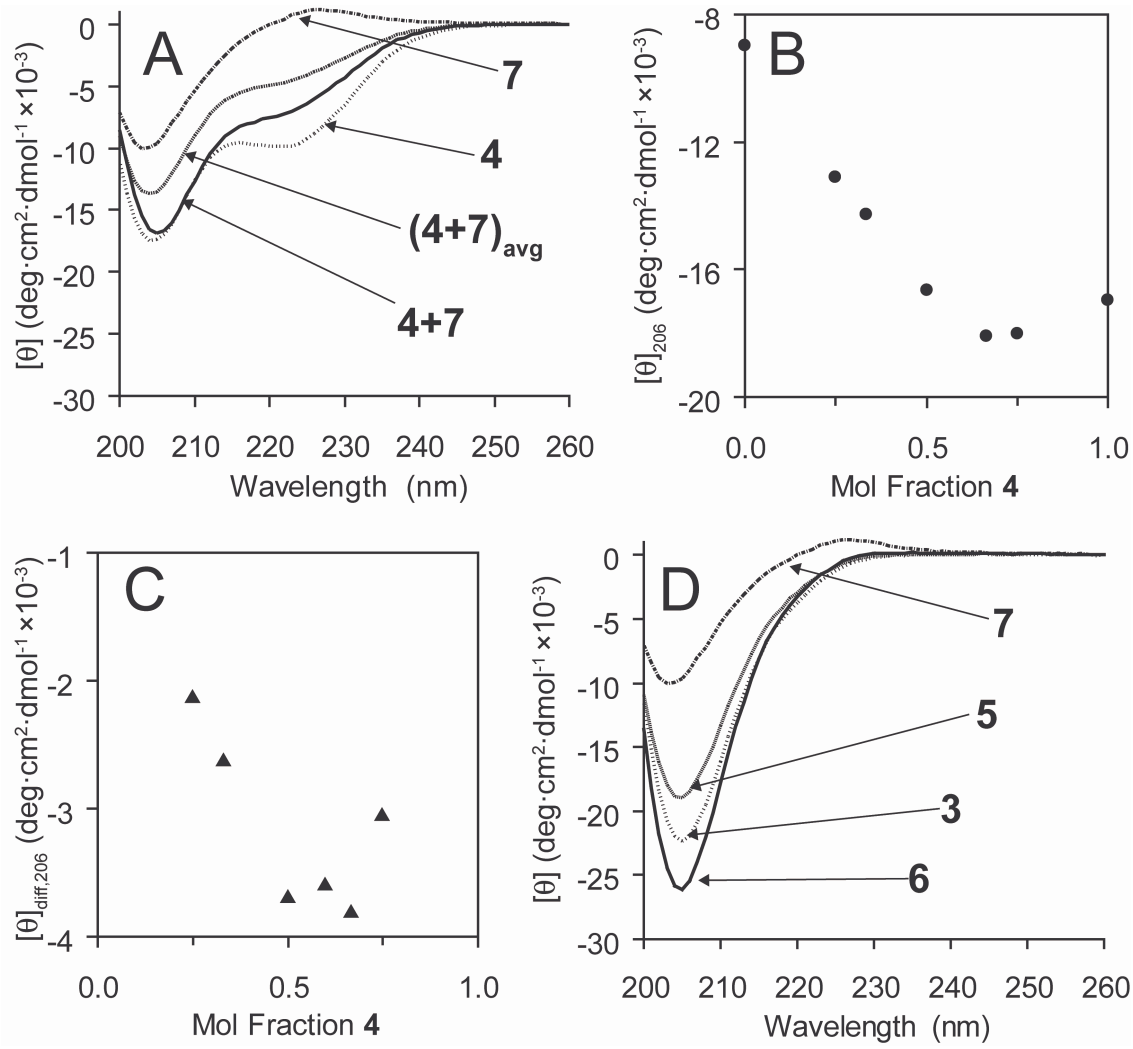

Figure S6. (A) CD spectra of 100 μM α-peptide **4**, 100 μM α/β-peptide **7**, and 50 μM **4** + 50 μM **7** (**4+7**) in PBS at 25 °C. $\mathbf{(4+7)_{avg}}$ is the average of the CD spectra of **4** alone plus **7** alone. The spectrum for **4+7** is moderately more intense than $\mathbf{(4+7)_{avg}}$, but much lower in intensity than the spectra of the other α-peptide + α/β-peptide pairs investigated here. These results suggest a diminished degree of helical association between **4** and **7** relative to the other peptide pairs. (B) Job plot of $[\theta]_{206}$ for 100 μM solutions differing in relative amounts of **4** and **7**. The lack of a distinct minimum makes it difficult to identify stoichiometry of the assembly. (C) Job plot of the difference between the observed $[\theta]_{206}$ and the weighted average $[\theta]_{206}$ for each mixture of **4** and **7**. Again, the lack of a distinct minimum makes it difficult to identify the stoichiometry of the assembly. (D) Comparison of the CD spectra of α/β-peptides **3**, **5**, **6**, and **7**. The spectrum of **7** is has a weak minimum near 203 nm, and a weak maximum near 226 nm, which is not consistent with the spectra of **3**, **5**, and **6** (for interpretation of CD data from helical α/β-peptides, see ref. S2). These features and the diminished intensity of the CD spectrum of **7** relative to that of **3**, **5**, and **6** suggest that cyclic APC residues contribute to α/β-peptide helical conformational stability. The increased intensity of the spectra of **3** and **6** relative to that of **5** suggests that Leu and β^3-hLeu may have greater helical propensities in α/β-peptides than Asn and β^2-hLeu, respectively.

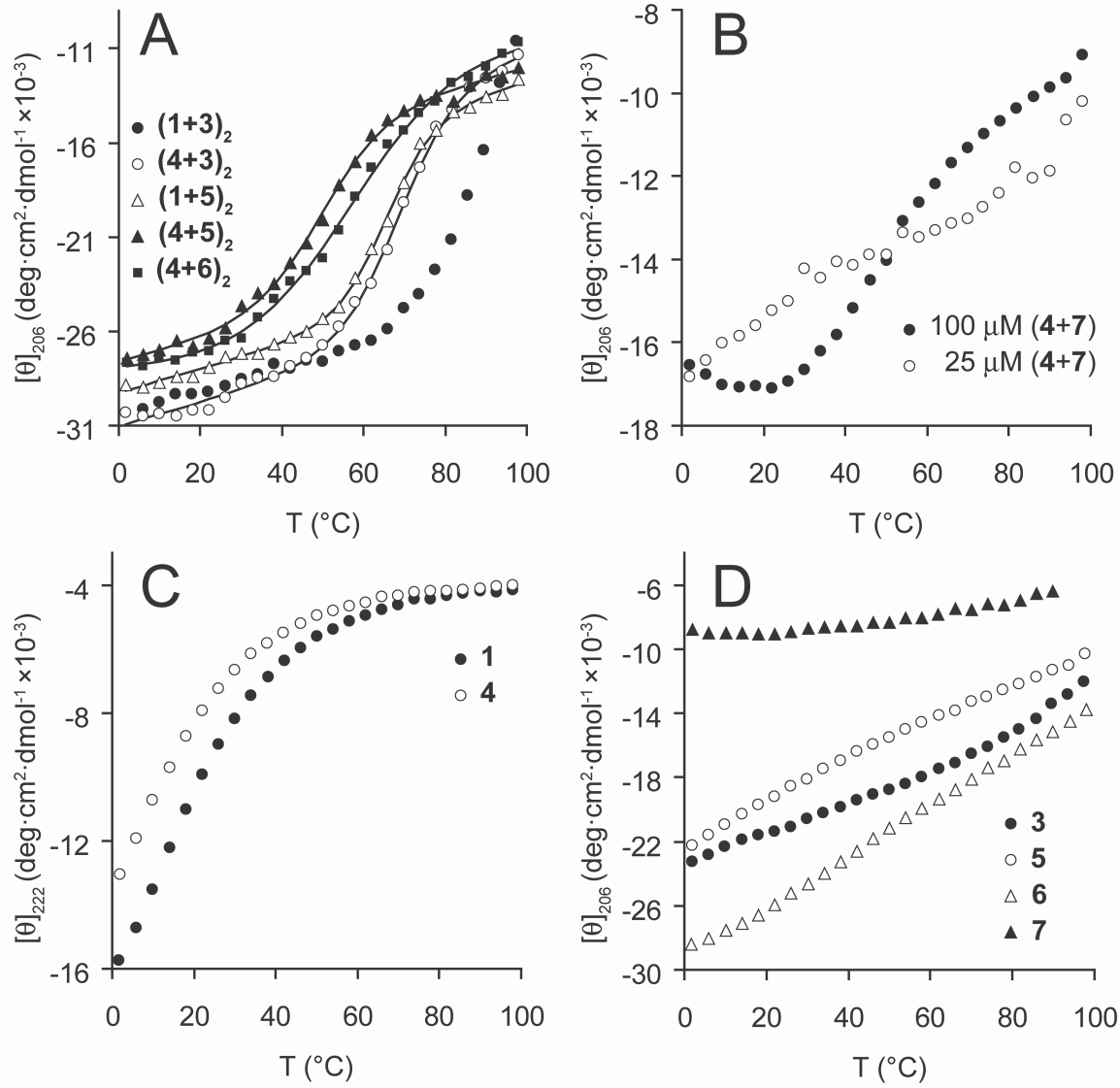

Figure S7. (A) Variable temperature CD at 25 μM total peptide in PBS for tetramers **(1+3)$_2$**, **(4+3)$_2$**, **(1+5)$_2$**, **(4+5)$_2$**, and **(4+6)$_2$**. Variation in the low temperature baselines for these peptides suggests the possibility of an additional thermal transition at 25 μM that is not present in the 100 μM data set. However, the 25 μM data were fit to a two-state denaturation model to facilitate comparison with the 100 μM data set. Solid lines represent the fits from which T_m values were obtained. (B) Variable temperature CD for the 1:1 mixture of **4** and **7** at 100 and 25 μM total peptide. The low temperature data for **4+7** at 100 μM present an irregular baseline and preclude fitting the data to a two-state denaturation model. The magnitude of this baseline is significantly smaller than that of the baselines of the tetramers shown in Figure 2 of the main text, suggesting a fundamental difference in "folded" states. The variable temperature data at 25 μM do not exhibit a cooperative unfolding transition. (C) Variable temperature CD data for α-peptides **1** and **4** at 100 μM in PBS showing cooperative unfolding transitions at low temperature. (D) Variable temperature CD data for α/β-peptides **3**, **5**, **6**, and **7**. These peptides do not exhibit cooperative unfolding transitions

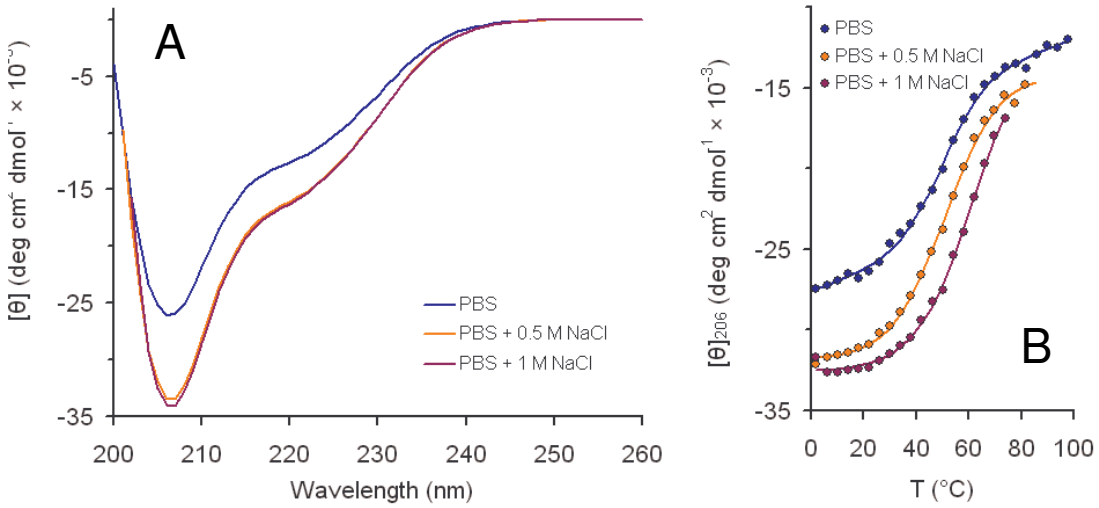

Figure S8. (A) CD spectra of 50 μM **4** + 50 μM **5** (**4**+**5**)$_2$ in PBS (blue), PBS + 0.5 M NaCl (orange), and PBS + 1.0 M NaCl (purple) at 25 °C. The CD spectrum of (**4**+**5**)$_2$ is more intense in PBS + NaCl than in PBS alone, suggesting that salt promotes the either the individual helical folding of **4** and **5** or the interaction of **4** with **5**, or some combination of these effects (for interpretation of CD data from helical α/β-peptides, see ref. S2). (B) Variable temperature CD for the 1:1 mixture of **4** and **5** (**4**+**5**)$_2$ at 25 μM total peptide in PBS (blue), PBS + 0.5 M NaCl (orange), and PBS + 1.0 M NaCl (purple). The increased stability of (**4**+**5**)$_2$ in the presence of increasing concentrations of salt is consistent with our hypothesis that the association between **4** and **5** is driven primarily by hydrophobic rather than electrostatic interactions.

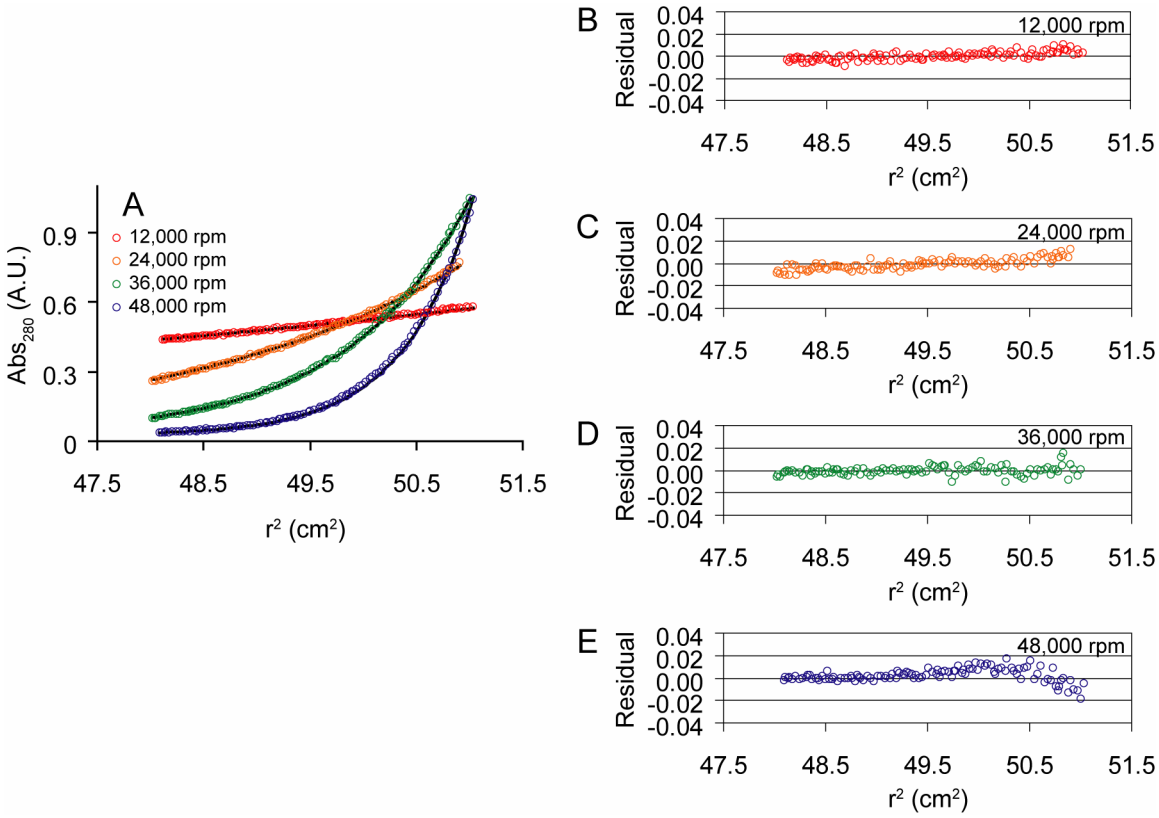

Figure S9. Analytical ultracentriguation data for $\mathbf{(1+3)_2}$. (A) Experimental AU data for 50 μM **1** + 50 μM **3** in PBS at 25 °C at 12,000 rpm, 24,000 rpm, 36,000 rpm, and 48,000 rpm. Solid lines show the calculated curves from a global fit of the data to a single species model with molecular weight of 13320 g·mol^{-1}, which is consistent with the predicted molecular weight of the $\mathbf{(1+3)_2}$ heterotetramer (13861 g·mol^{-1}, 4.6% difference). Residuals between observed and calculated data are plotted for each speed: (B) 12,000 rpm, (C) 24,000 rpm, (D) 36,000 rpm, and (E) 48,000 rpm.

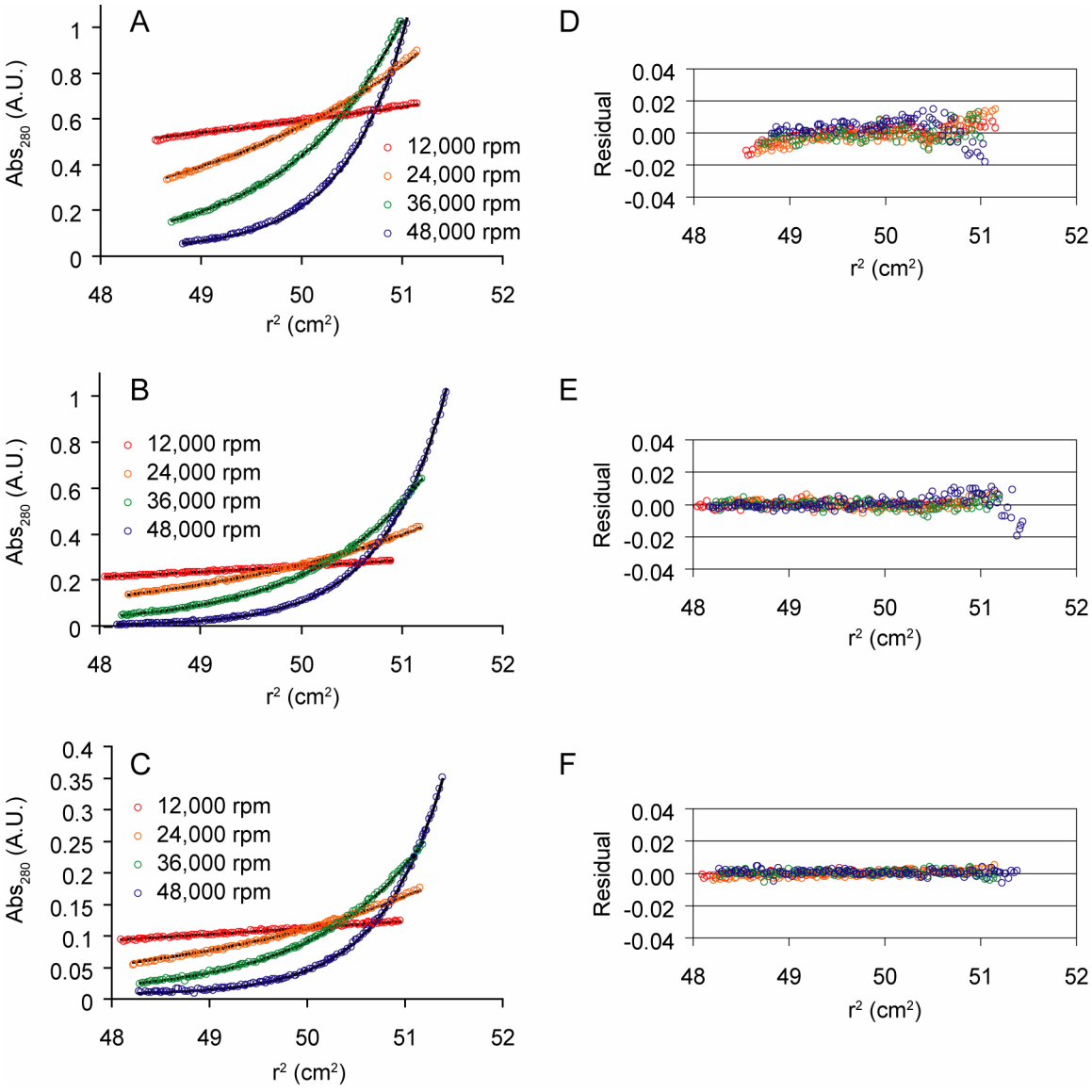

Figure S10. Analytical ultracentriguation data for **(4+3)$_2$**. Experimental AU data for (A) 50 μM **4** + 50 μM **3**, (B) 25 μM **4** + 25 μM **3**, and (C) 12.5 μM **4** + 12.5 μM **3** in PBS at 25 °C and at 12,000 rpm, 24,000 rpm, 36,000 rpm, and 48,000 rpm. Solid lines show the calculated curves from a global fit of the data to a single species model with molecular weight of 13380 g·mol^{-1}, which is consistent with the predicted molecular weight of the **(4+3)$_2$** heterotetramer (13863 g·mol^{-1}, 3.5% difference). Residuals between observed and calculated data are plotted for each concentration: (D) 50 μM **4** + 50 μM **3**, (E) 25 μM **4** + 25 μM **3**, and (F) 12.5 μM **4** + 12.5 μM **3**.

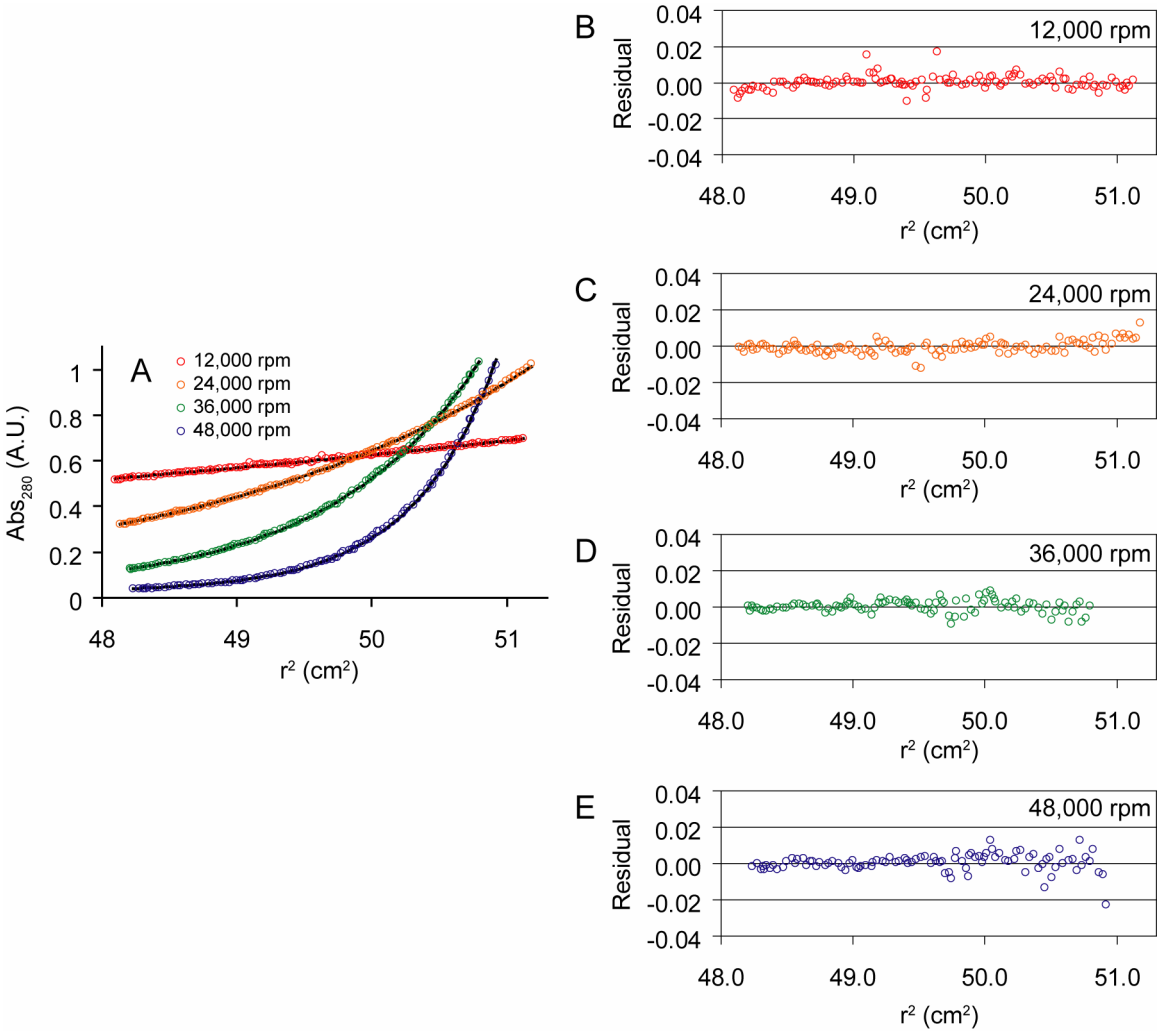

Figure S11. Analytical ultracentriguation data for **(1+5)$_2$**. (A) Experimental AU data for 50 μM **1** + 50 μM **5** in PBS at 25 °C at 12,000 rpm, 24,000 rpm, 36,000 rpm, and 48,000 rpm. Solid lines show the calculated curves from a global fit of the data to a single species model with molecular weight of 13350 g·mol^{-1}, which is consistent with the predicted molecular weight of the **(1+5)$_2$** heterotetramer (13863 g·mol^{-1}, 3.7% difference). Residuals between observed and calculated data are plotted for each speed: (B) 12,000 rpm, (C) 24,000 rpm, (D) 36,000 rpm, and (E) 48,000 rpm.

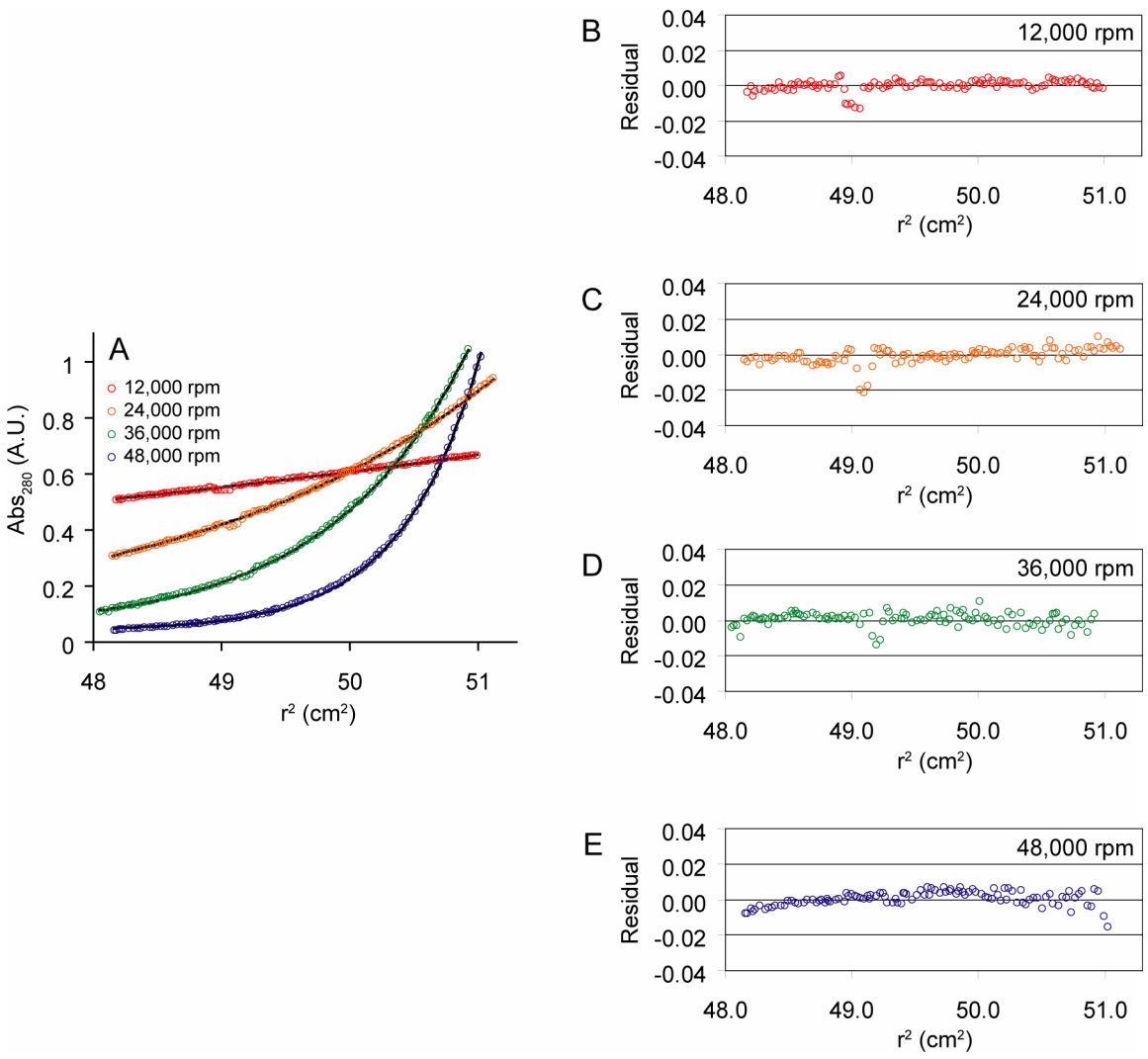

Figure S12. Analytical ultracentriguation data for **(4+5)$_2$**. (A) Experimental AU data for 50 μM **4** + 50 μM **5** in PBS at 25 °C at 12,000 rpm, 24,000 rpm, 36,000 rpm, and 48,000 rpm. Solid lines show the calculated curves from a global fit of the data to a single species model with molecular weight of 13480 g·mol^{-1}, which is consistent with the predicted molecular weight of the **(4+5)$_2$** heterotetramer (13864 g·mol^{-1}, 2.8% difference). Residuals between observed and calculated data are plotted for each speed: (B) 12,000 rpm, (C) 24,000 rpm, (D) 36,000 rpm, and (E) 48,000 rpm.

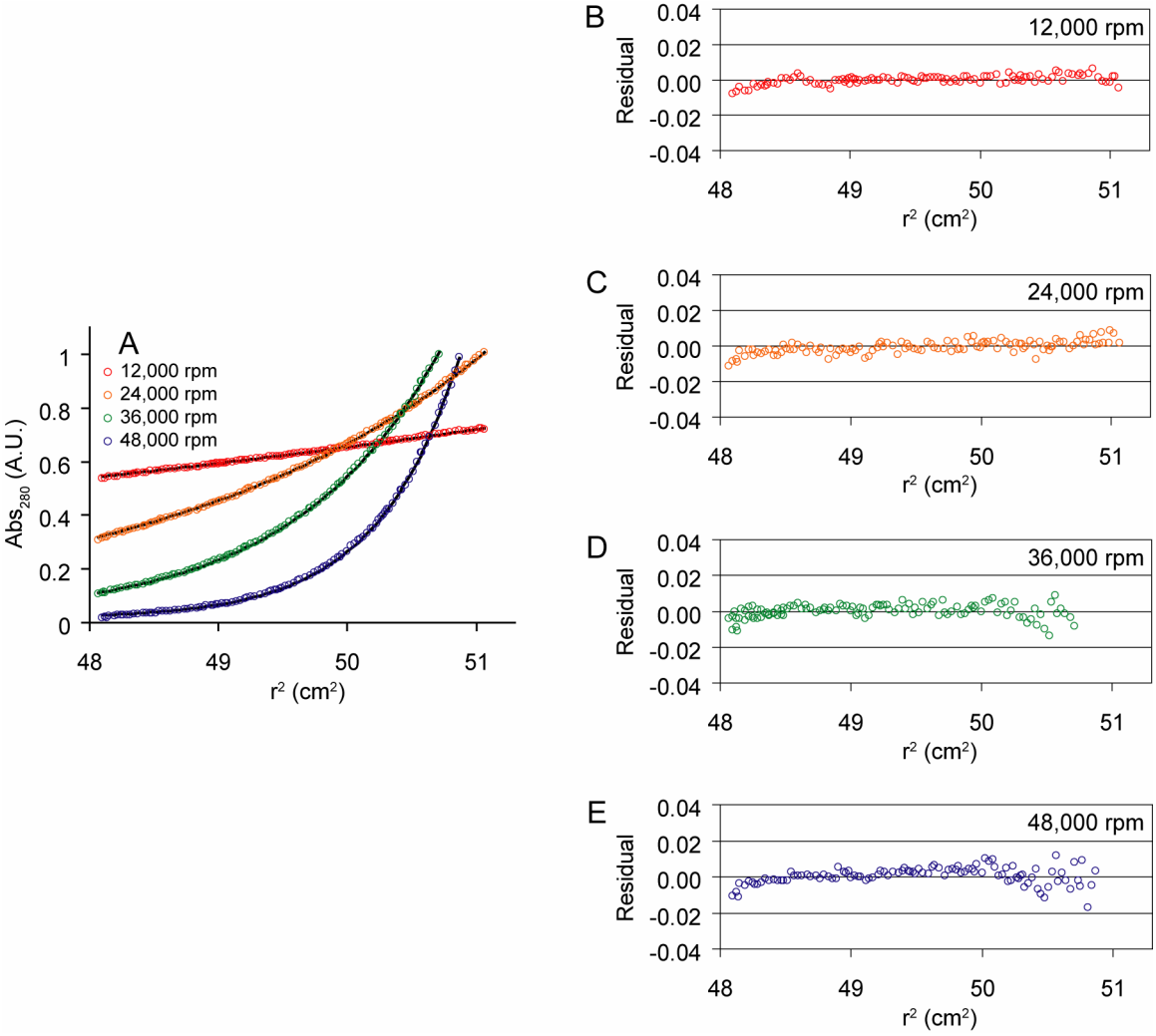

Figure S13. Analytical ultracentriguation data for **(4+6)$_2$**. (A) Experimental AU data for 50 μM **4** + 50 μM **6** in PBS at 25 °C at 12,000 rpm, 24,000 rpm, 36,000 rpm, and 48,000 rpm. Solid lines show the calculated curves from a global fit of the data to a single species model with molecular weight of 13050 g·mol^{-1}, which is consistent with the predicted molecular weight of the **(4+6)$_2$** heterotetramer (13864 g·mol^{-1}, 5.7% difference). Residuals between observed and calculated data are plotted for each speed: (B) 12,000 rpm, (C) 24,000 rpm, (D) 36,000 rpm, and (E) 48,000 rpm.

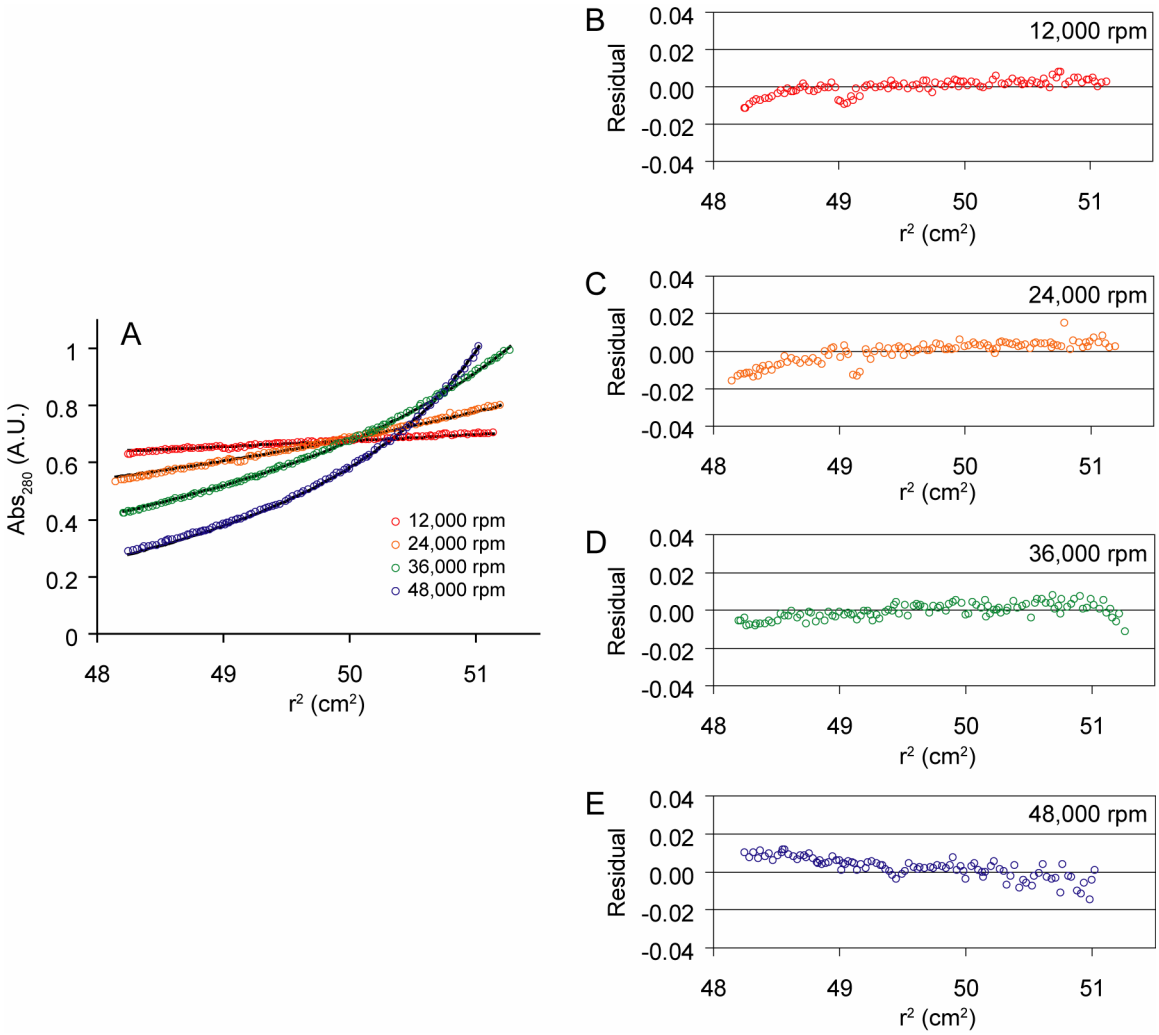

Figure S14. Analytical ultracentriguation data for the 1:1 mixture of **4+7**. (A) Experimental AU data for 50 μM **4** + 50 μM **7** in PBS at 25 °C at 12,000 rpm, 24,000 rpm, 36,000 rpm, and 48,000 rpm. Solid lines show the calculated curves from a global fit of the data. The best fit of the data was based on an equilibrium model, in which the monomer molecular weight was held constant (at the average molecular weight of **4** and **7** = 3281 g·mol^{-1}) and the equilibrium constant and aggregation number were allowed to float. In the fit shown here, n = 4.5, and K = 0.40. Residuals between observed and calculated data are plotted for each speed: (B) 12,000 rpm, (C) 24,000 rpm, (D) 36,000 rpm, (E) 48,000 rpm. The non-integral value of the aggregation number and the systematic deviation of the residuals from zero suggest that the system is more complicated than the model presented here. However, **4** and **7** clearly do not associate to form a 2:2 heterotetramer, and the small size of the equilibrium constant suggests that the dominant species in the μM range is monomer (>90%), which is consistent with Job plot and variable temperature CD results for **4+7** (see Figures S6 and S7).

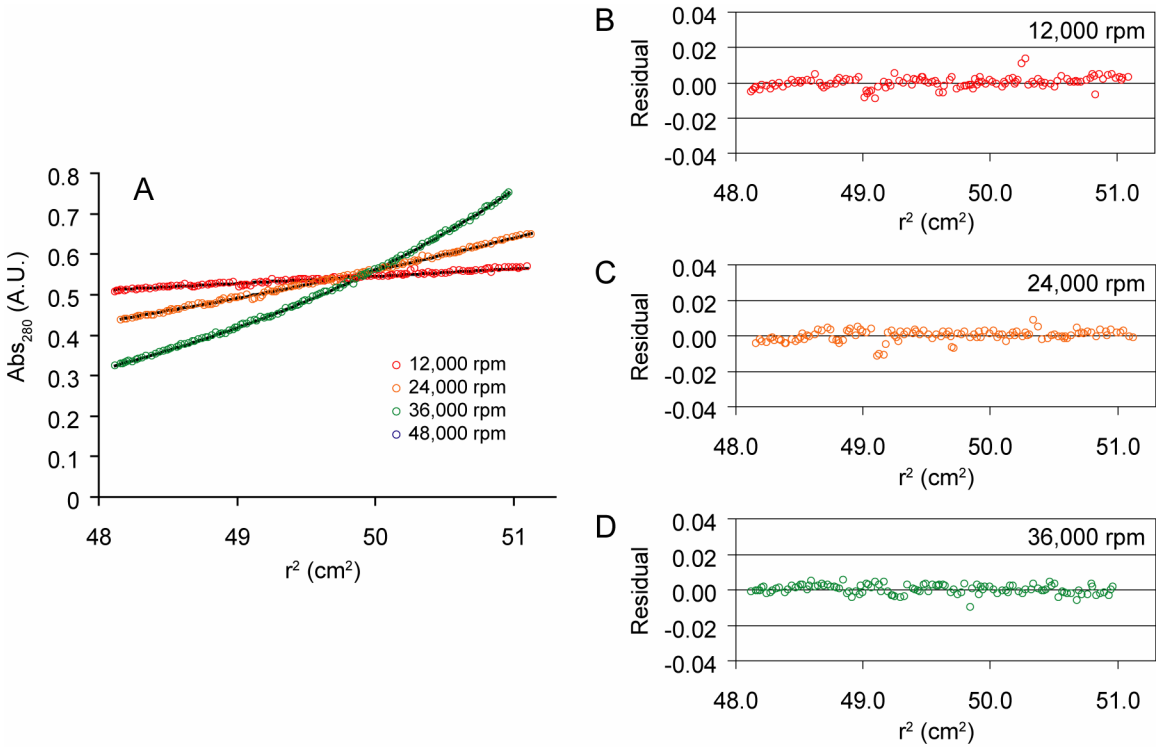

Figure S15. Analytical ultracentriguation data for the α-peptide **1**. (A) Experimental AU data for 100 μM **1** in PBS at 25 °C at 12,000 rpm, 24,000 rpm, and 36,000 rpm. Solid lines show the calculated curves from a global fit of the data. The best fit of the data was based on an equilibrium model, in which the monomer molecular weight was held constant (at 3559 g·mol^{-1}) and the equilibrium constant and aggregation number were allowed to float. In the fit shown here, n = 2.2, and K = 0.27, suggesting a monomer-dimer equilibrium in which ~85% of the peptide exists as monomer in the μM range. These observations are in rough agreement with the results of Kim et al. (ref S1) who use a monomer-dimer-tetramer equilibrium to describe the sedimentation behavior of **1** (in their model, ~80% of the peptide is present as monomer, 18% as dimer, and 2% as tetramer). Whatever its precise aggregation behavior, **1** clearly does not form a significant amount of tetramer by itself, in contrast to its behavior in the presence of **3** or **5**. Residuals between observed and calculated data are plotted for each speed: (B) 12,000 rpm, (C) 24,000 rpm, and (D) 36,000 rpm.

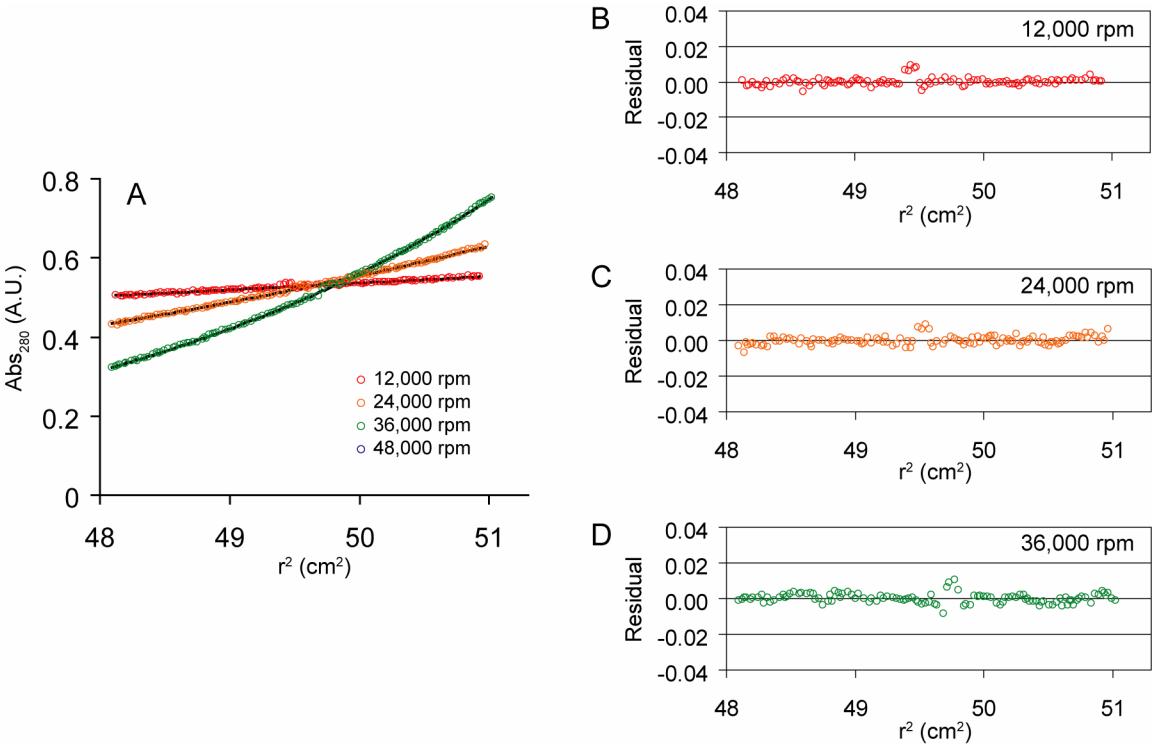

Figure S16. Analytical ultracentriguation data for the α-peptide **4**. (A) Experimental AU data for 100 μM **4** in PBS at 25 °C at 12,000 rpm, 24,000 rpm, and 36,000 rpm. Solid lines show the calculated curves from a global fit of the data to a single species model with molecular weight of 3761 g·mol^{-1}, which is consistent with the molecular weight of **4** (3560 g·mol^{-1}, 5.7% difference). Residuals between observed and calculated data are plotted for each speed: (B) 12,000 rpm, (C) 24,000 rpm, and (D) 36,000 rpm.

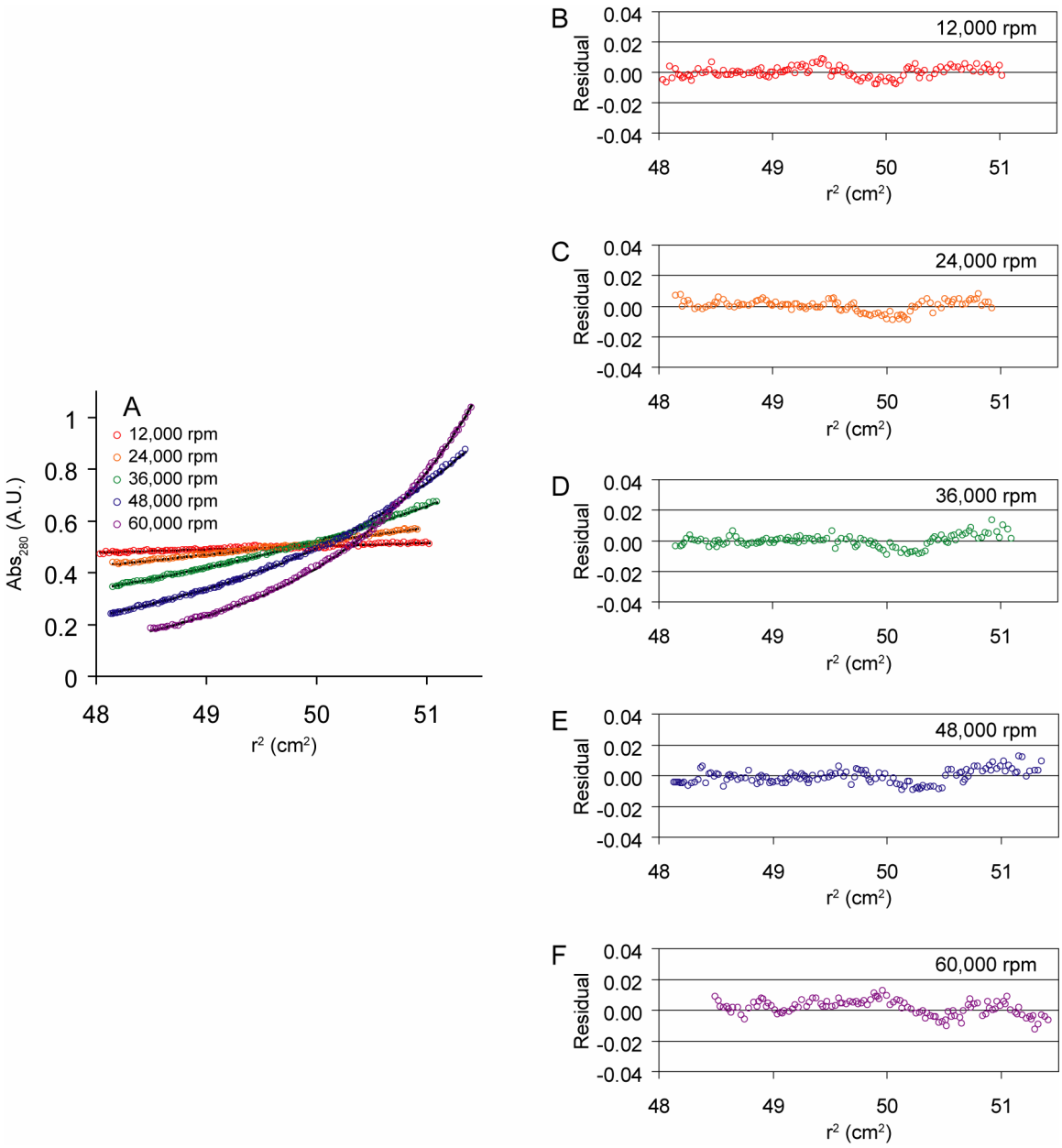

Figure S17. Analytical ultracentriguation data for the α/β-peptide **3**. (A) Experimental AU data for 100 μM **3** in PBS at 25 °C at 12,000 rpm, 24,000 rpm, 36,000 rpm, 48,000 rpm, and 60,000 rpm. Solid lines show the calculated curves from a global fit of the data. The best fit of the data was based on an equilibrium model, in which the monomer molecular weight was held constant (at 3371 g·mol^{-1}) and the equilibrium constant and aggregation number were allowed to float. In the fit shown here, n = 2.4, and K = 0.47, suggesting a monomer-dimer equilibrium in which ~79% of the peptide exists as monomer in the μM range. Whatever its precise aggregation behavior, **3** clearly does not form a significant amount of tetramer by itself, in contrast to its behavior in the presence of **1** or **4**. Residuals between observed and calculated data are plotted for each speed: (B) 12,000 rpm, (C) 24,000 rpm, (D) 36,000 rpm, (E) 48,000 rpm, and (F) 60,000 rpm.

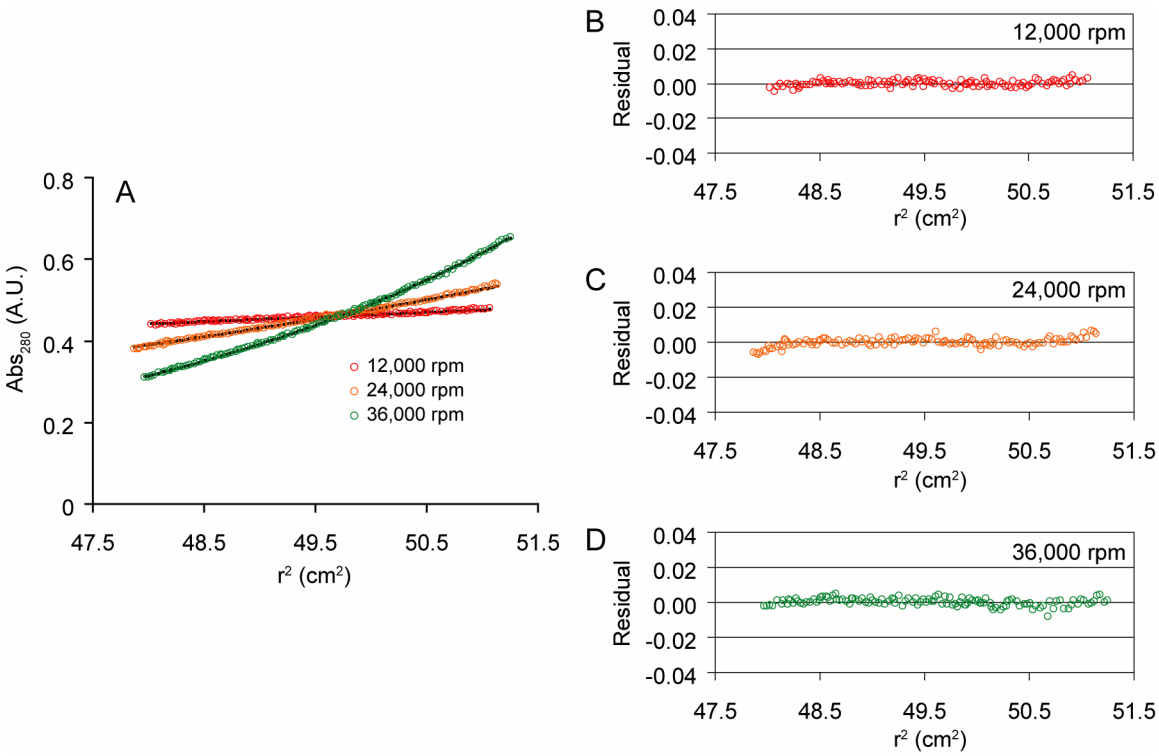

Figure S18. Analytical ultracentriguation data for the α/β-peptide **5**. (A) Experimental AU data for 100 μM **5** in PBS at 25 °C at 12,000 rpm, 24,000 rpm, and 36,000 rpm. Solid lines show the calculated curves from a global fit of the data. The best fit of the data was based on an equilibrium model, in which the monomer molecular weight was held constant (at 3372 g·mol^{-1}) and the equilibrium constant and aggregation number were allowed to float. In the fit shown here, n = 1.8, and K = 0.44, suggesting a monomer-dimer equilibrium in which ~76% of the peptide exists as monomer in the μM range. Whatever its precise aggregation behavior, **5** clearly does not form a significant amount of tetramer by itself, in contrast its in the presence of **1** or **4**. Residuals between observed and calculated data are plotted for each speed: (B) 12,000 rpm, (C) 24,000 rpm, and (D) 36,000 rpm.

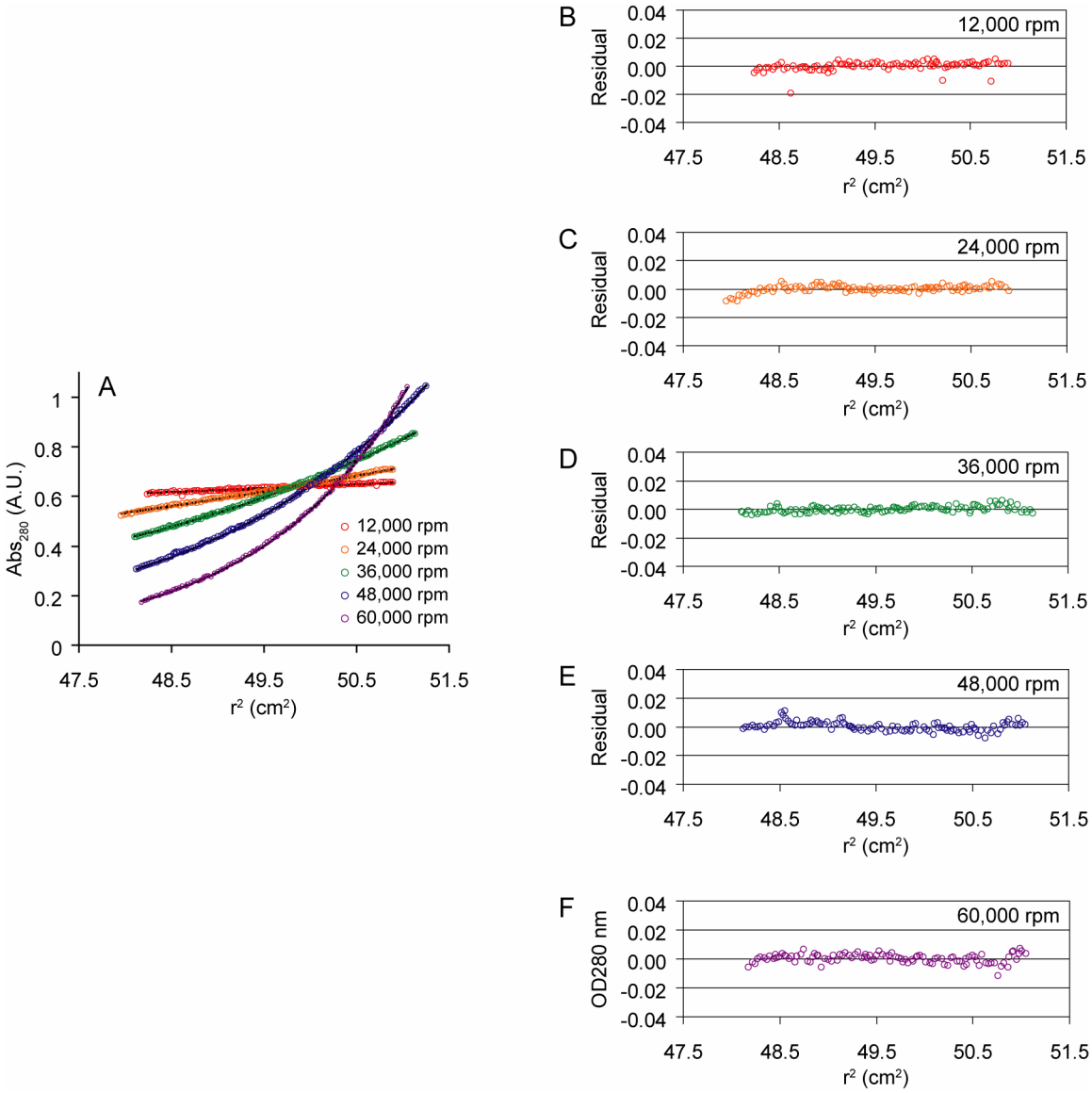

Figure S19. Analytical ultracentriguation data for the α/β-peptide **6**. (A) Experimental AU data for 100 μM **6** in PBS at 25 °C at 12,000 rpm, 24,000 rpm, 36,000 rpm, 48,000 rpm, 60,000 rpm. Solid lines show the calculated curves from a global fit of the data to a single species model with molecular weight of 3768 g·mol^{-1}, which is 12% higher than the molecular weight of **6** (3372 g·mol^{-1}). This difference suggests the possible presence of another species in equilibrium with monomeric **6**, but attempts to fit the data to equilibrium models did not improve the fit by decreasing the magnitude or randomness of the deviation of the residuals from zero. Whatever its precise aggregation behavior, **6** clearly does not form a tetramer on its own, in contrast to its behavior in the presence of **4**. Residuals between observed and calculated data are plotted for each speed: (B) 12,000 rpm, (C) 24,000 rpm, (D) 36,000 rpm, (E) 48,000 rpm, and (F) 60,000 rpm.

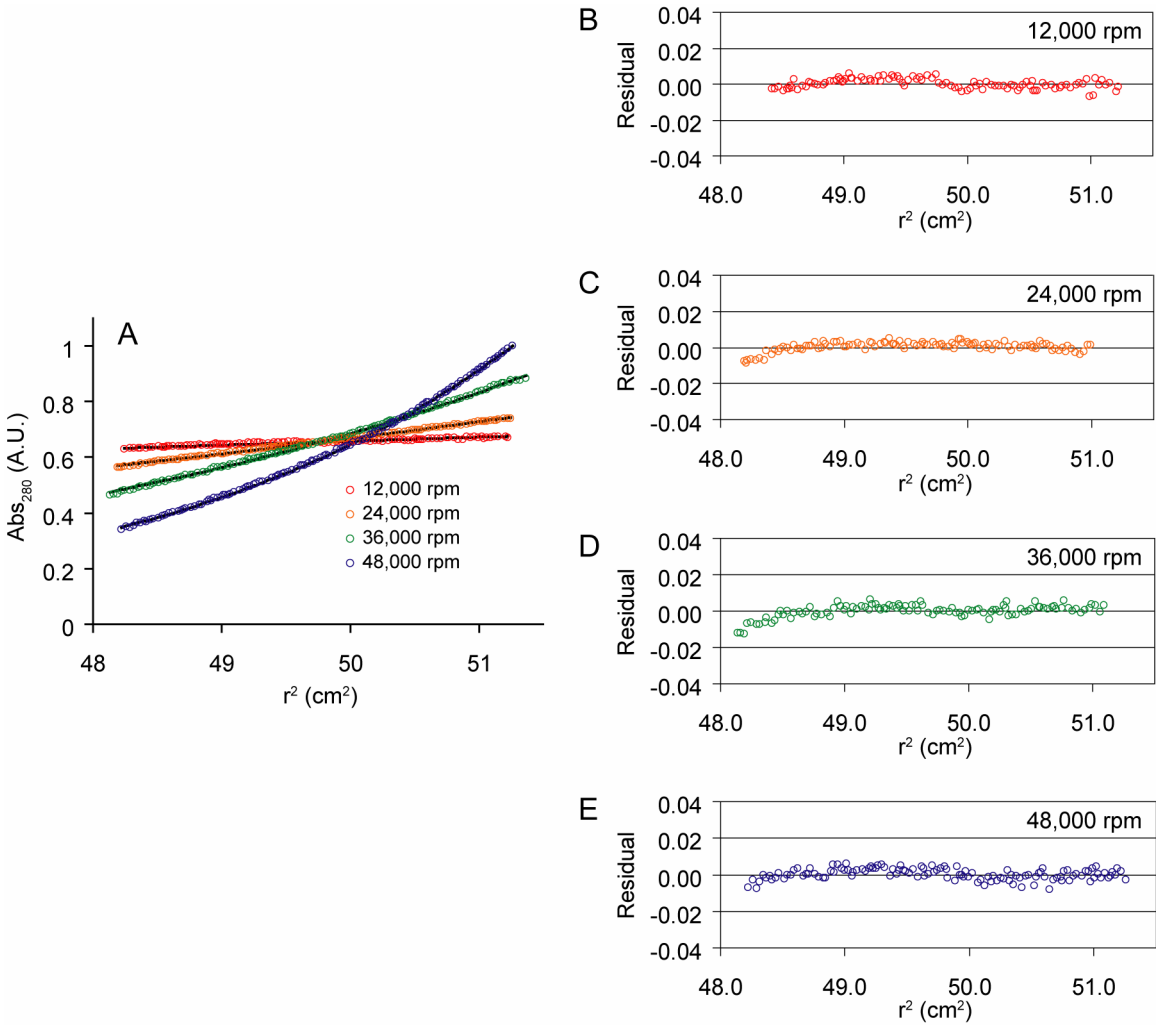

Figure S20. Analytical ultracentriguation data for the α/β-peptide **7**. (A) Experimental AU data for 100 μM **7** in PBS at 25 °C at 12,000 rpm, 24,000 rpm, 36,000 rpm, and 48,000 rpm. Solid lines show the calculated curves from a global fit of the data to a single species model with molecular weight of 4024 g·mol^{-1}, which is 13% higher than the molecular weight of **7** (3553 g·mol^{-1}). This difference suggests the possible presence of another species in equilibrium with monomeric **7**, but attempts to fit the data to equilibrium models did not improve the fit by decreasing the magnitude or randomness of the deviation of the residuals from zero. Whatever its precise aggregation behavior, **7** clearly does not form a tetramer on its own. Residuals between observed and calculated data are plotted for each speed: (B) 12,000 rpm, (C) 24,000 rpm, (D) 36,000 rpm, and (E)

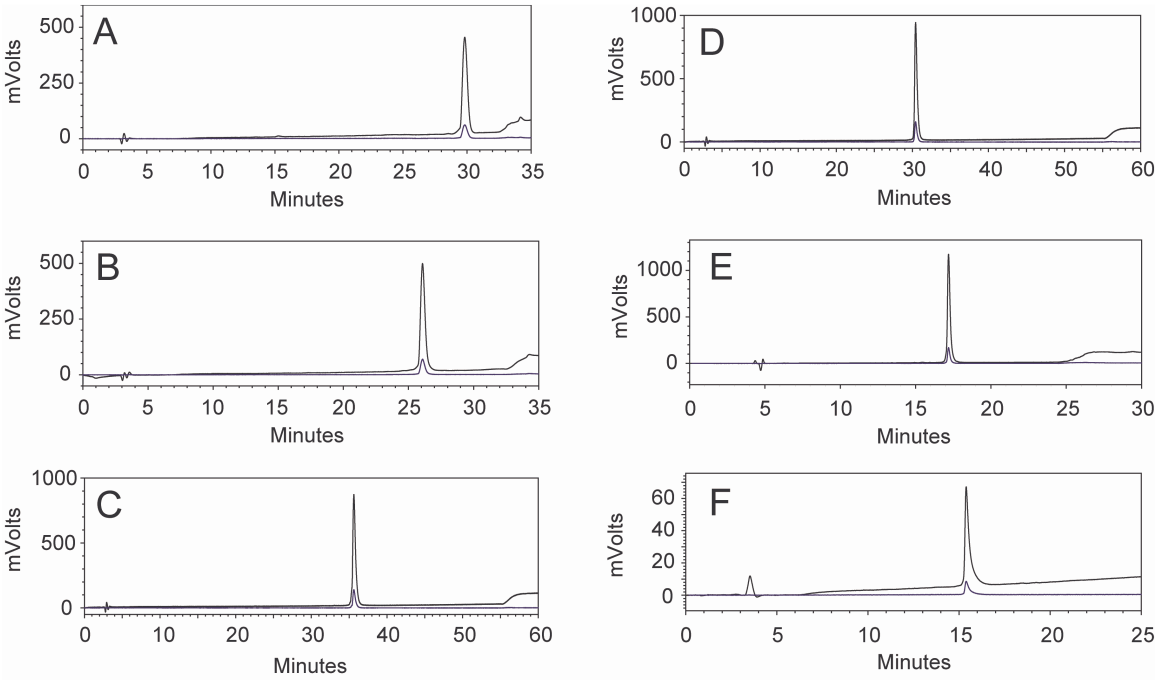

Figure S21. Purity of purified α-peptides and α/β-peptide foldamers was analyzed by reverse-phase HPLC. Peptides were eluted using linear gradients of water (solvent A) in acetonitrile (solvent B) with 0.1% trifluoroacetic acid and were detected by monitoring absorbance at 220 nm (black) and near 280 nm (blue). (A) HPLC chromatogram of α-peptide **1** on a C18 analytical column, using the following gradient: 10% to 60% solvent B over 25 minutes, followed by 5 minutes at 95% B, then 5 minutes at 10% B. (B) HPLC chromatogram of α-peptide **4** on a C18 analytical column, using the following gradient: 10% to 60% solvent B over 25 minutes, followed by 5 minutes at 95% B, then 5 minutes at 10% B. (C) HPLC chromatogram of α-peptide **1** on a C18 analytical column, using the following gradient: 10% to 60% solvent B over 25 minutes, followed by 5 minutes at 95% B, then 5 minutes at 10% B. (C) HPLC chromatogram of α/β-peptide **3** on a C18 analytical column, using the following gradient: 10% to 60% solvent B over 50 minutes, followed by 5 minutes at 95% B, then 5 minutes at 10% B. (D) HPLC chromatogram of α/β-peptide **5** on a C18 analytical column, using the following gradient: 10% to 60% solvent B over 50 minutes, followed by 5 minutes at 95% B, then 5 minutes at 10% B. (E) HPLC chromatogram of α/β-peptide **6** on a C18 semiprep column, using the following gradient: 20% to 40% solvent B over 20 minutes, followed by 5 minutes at 95% B, then 5 minutes at 20% B. (F) HPLC chromatogram of α/β-peptide **7** on a C18 monomeric analytical column, using the following gradient: 20% to 40% solvent B over 20 minutes, followed by 5 minutes at 95% B. Based on these data we estimate the purity of each peptide to be > 95%.

Peptide Synthesis

Peptides were synthesized on solid phase using standard Fmoc chemistry, with amino acid activation by 2-(1H-Benzotriazole-1-yl)-1,1,3,3-tetramethyluronium hexafluorophosphate (HBTU) and N-Hydroxybenzotriazole (HOBt). Fmoc-protected α-amino acids with acid-labile side-chain protecting groups and polystyrene tentagel resin (NovaSyn TGR) were purchased from Novabiochem. Fmoc-β^2-homoleucine,[S3] Fmoc-ACPC,[S4] and Fmoc-APC(Boc)[S5] were synthesized as described previously. HBTU was purchased from AnaSpec. HOBt and N,N-diisopropylethylamine (DIEA) were purchased from Aldrich. Peptides were synthesized on solid phase using an automated peptide synthesizer (Applied Biosystems Synergy or Pioneer) or manually in a CEM MARS V multimode microwave.[S6]

A general protocol for microwave assisted manual peptide synthesis is as follows: 50 μmol resin was weighed into a fritted polypropylene tube and allowed to swell first in dichloromethane (CH_2Cl_2), then in N,N-dimethylformamide (DMF). For coupling of an activated amino acid to an unprotected amine on resin: The desired Fmoc-protected amino acid (150 μmol, 3 eq) was dissolved by vortexing in 2.2 ml DMF and 300 μl of 0.5 M HBTU in DMF. To the dissolved amino acid solution were added 300 μl each of 0.5 M HOBt and 1.0 M DIEA. This mixture was vortexed briefly, and allowed to react for at least 1 minute. The activated amino acid solution was then added to the fritted polypropylene tube containing the resin. The resin was heated to 70 °C in the microwave (2 minute ramp to 70 °C, 4 minute hold at 70 °C) with stirring. Following the coupling reaction, the resin was removed from the microwave, and the activated amino acid solution was drained from the resin with a vacuum manifold. The resin was rinsed three times with DMF, three times with CH_2Cl_2, and three times again with DMF. To deprotect the amine on the newly coupled amino acid, 3 ml of 20% piperidine in DMF were added to the resin, and the resin was heated to 80 °C in the microwave (2 minute ramp to 80 °C, 2 minute hold at 80 °C) with stirring. Following the deprotection reaction, the resin was rinsed three times with DMF, three times with CH_2Cl_2, and three times again with DMF.

The cycles of coupling and deprotection were alternately repeated to give the desired full length peptide. Following the final deprotection cycle, the N-terminal amine was acetylated by stirring the resin in a 14:5:1 mixture of CH_2Cl_2, acetic anhydride, and triethylamine for at least 30 min. Acetylated peptides were globally deprotected and cleaved from the resin by stirring the resin in 95% trifluoroacetic acid (TFA), 2.5% water, and 2.5% triisopropylsilane for 2 to 4 hours. Following the cleavage reaction, the TFA solution was drained from the resin, and concentrated under N_2. Peptides were precipitated from the concentrated TFA solution with diethyl ether. Following centrifugation, the ether was decanted and the peptide pellet was washed with diethyl ether. The washed peptide pellet was dried under N_2 and stored at 4 °C until purification. Immediately prior to purification, the peptide was dissolved in 1:1 water/acetonitrile. Peptides were purified by reverse-phase HPLC using a linear gradient of water and acetonitrile with 0.1% TFA. HPLC fractions containing the desired peptide product were pooled, frozen, and lyophilized. Peptide identity was confirmed by matrix-assisted laser desorption/ionization time-of-flight spectrometry (MALDI-TOF, see Table S1) and purity was confirmed by analytical HPLC (see Figure S20).

Table S1. MALDI-TOF data and calculated $\bar{v}$ for α-peptides and α/β-peptide foldamers

Peptide	calculated $[M+H]^+$ ($g \cdot mol^{-1}$)	observed $[M+H]^+$ ($g \cdot mol^{-1}$)	calculated $\bar{v}$ ($cm^3 \cdot g^{-1}$)
1	3562.9	3563.4	0.738
3	3359.2	3359.8	0.801
4	3563.9	3564.2	0.730
5	3360.2	3360.4	0.792
6	3360.2	3360.2	0.792
7	3540.4	3540.3	0.827

Circular Dichroism Spectroscopy

Measurements were made with an Aviv 62A DS Circular Dichroism Spectrometer, using quartz cuvettes with a 0.1 cm path length. Peptide solutions were prepared in phosphate buffered saline (PBS, pH 7) and peptide concentrations were determined spectroscopically based on tryptophan absorbance at 280 nm. CD spectra were obtained by monitoring molar ellipticity from 260 to 200 nm, with 5 second averaging times. Spectra were corrected for baseline molar ellipticity at 260 nm. Job analysis was performed by obtaining the CD spectra of PBS solutions of combinations of the α-peptide and α/β-peptide foldamers in varying ratios, but constant total peptide concentration. Variable temperature CD data were obtained by monitoring molar ellipticity at 206 nm from 2 to 98 °C at 4°C intervals, with 10 minute equilibration time between data points and 5 second averaging times. Except for the denaturations of 50 μM **1** + 50 μM **3** [$(\mathbf{1+3})_2$] and 50 μM **4** + 50 μM **3** [$(\mathbf{4+3})_2$], which did not reach fully unfolded baselines, thermal denaturation curves were well described by equation S1:

$$[\theta] = c_0 + c_1 \cdot x + \frac{c_2}{1 + \exp(-\frac{x - T_m}{c_3})} \qquad \text{(S1)}$$

where [θ] is molar ellipticity in $deg \cdot cm^2 \cdot dmol^{-1}$, x is temperature in Kelvin, T_m is the melting temperature of the unfolding transition in Kelvin, and c_0, c_1, c_2, and c_3 are parameters of the fit (in some cases, a better fit was obtained by setting $c_1 = 0$).

Analytical Ultracentrifugation

Sedimentation equilibrium experiments were performed using a Beckman XLA ultracentrifuge. Peptides were loaded into 1.2 cm cells, and sedimentation was monitored by absorbance at 280 nm. Sedimentation equilibria were analyzed at several speeds ranging from 12 to 60 krpm, and data were collected at 0.001 cm intervals along the length of the cell at each speed. After changing speeds, data collection was repeated every 2 hours until consecutive data sets were superimposable. Apparent molecular weight was determined by non-linear regression of the equilibrium radial absorbance data using the program SigmaPlot (SPSS, Inc.). Data were fit to models either for a single species, or for equilibrium between monomer and *n*-mer (equations S2 and S3, respectively):

$$c_r = c_{base} + c_{ref} \exp\left[\frac{M(1-\bar{v}\rho)\omega^2}{2RT}(r^2 - r_{ref}^2)\right] \quad \text{(S2)}$$

$$c_r = c_{base} + c_1 \exp\left[\frac{M_1(1-\bar{v}\rho)\omega^2}{2RT}(r^2 - r_{ref}^2)\right] + Kc_1^n\left[\frac{nM_1(1-\bar{v}\rho)\omega^2}{2RT}(r^2 - r_{ref}^2)\right] \quad \text{(S3)}$$

In equation S2, c_r is the concentration of peptide (in absorbance units) at radial position r (in cm), c_{ref} is the concentration of peptide at an arbitrary reference radial position r_{ref}, M is the apparent molecular weight of the peptide, $\bar{v}$ is the partial specific volume of the peptide (in $cm^3 \cdot g^{-1}$), ρ is the density of the sample, ω is the radial velocity (in s^{-1}) during the measurement, R is the universal gas constant, T is the temperature (in Kelvin), and c_{base} is a correction for baseline absorbance resulting from non-sedimenting components of the sample. The variables in equation S3 have the same meaning, except c_1 is the concentration of the monomer (in absorbance units), K is the equilibrium constant for the association between the monomer and the n-mer, n is the aggregation number for the species in equilibrium with the monomer, and M_1 is the molecular weight of the monomer. The partial specific volumes for each peptide were calculated according to the method of Durchschlag and Zipper[S7] and are shown in Table S1.

References for Supporting Information

(S1) Lumb, K. J.; Kim, P. S. *Biochemistry* **1995**, *34*, 8642–8648.

(S2) Schmitt, M. A.; Weisblum, B.; Gellman, S. H. *J. Am. Chem. Soc.* **2007**, *129*, 417–428.

(S3) (a) Chi, Y.; Gellman, S. H. *J. Am. Chem. Soc.* **2006**, *128*, 6084–6805. (b) Chi, Y.; English, E. P.; Pomerantz, W. C; Horne, W. S.; Joyce, L. A.; Alexander, L. R.; Fleming, W. S.; Hopkins, E. A.; Gellman, S. H. *J. Am. Chem. Soc.* **2007**, in press.

(S4) LePlae, P. R.; Umezawa, N; Lee, H. -S.; Gellman, S. H. *J. Org. Chem.* **2001**, *66*, 5629–5632.

(S5) Lee, H. -S.; LePlae, P. R.; Porter, E. A.; Gellman, S. H. *J. Org. Chem.* **2001**, *66*, 3597–3599.

(S6) Murray, J. K.; Gellman, S. H. *Org. Lett.* **2005**, *7*, 1517–1520.

(S7) Durchschlag, H.; Zipper, P. *Prog. Colloid Polym. Sci.* **1994**, *94*, 20–39.